J Oceanogr (2014) 70:389–403
DOI 10.1007/s10872-014-0237-5

SHORT CONTRIBUTION

# Origin of near-surface high-salinity water observed in the Kuroshio Extension region

**Akira Nagano · Kazuyuki Uehara · Toshio Suga · Yoshimi Kawai · Hiroshi Ichikawa · Meghan F. Cronin**

Received: 23 December 2013 / Revised: 9 May 2014 / Accepted: 13 May 2014 / Published online: 19 June 2014


**Abstract** Hydrographic data in the Kuroshio Extension (KE) region from 2008 to 2010 show large year-to-year variability in near-surface salinity, including a very large anomalous event in February 2010. During this event, the deep winter mixed layer in the southern KE region had higher salinity than had existed during the previous summer in September 2009. Our analysis shows that advection from the Philippine Sea along the western branch of the North Pacific subtropical gyre, taking approximately 9 months, resulted in this large salinity anomaly in February 2010 and contributes to the inter-annual salinity variability in the southern KE region.

**Keywords** Kuroshio Extension · Salinity · Sea surface buoy · Argo float · KEO · JKEO

A. Nagano (✉) · T. Suga · Y. Kawai · H. Ichikawa
Research and Development Center for Global Change, Japan Agency for Marine-Earth Science and Technology, 2-15 Natsushima-cho, Yokosuka, Kanagawa 237-0061, Japan
e-mail: nagano@jamstec.go.jp

K. Uehara
School of Marine Science and Technology, Tokai University, 3-20-1 Orido, Shimizu-ku, Shimizu 424-8610, Japan

T. Suga
Graduate School of Science, Tohoku University, 6-3 Aramkai-aza-aoba, Aoba-ku, Sendai 980-8578, Japan

M. F. Cronin
Pacific Marine Environmental Laboratory, National Oceanic and Atmospheric Administration, 7600 Sand Point Way NE, Seattle, WA 98115, USA

## 1 Introduction

By transporting and releasing heat to the atmosphere, the oceans play a critical role in the global climate system. Within the North Pacific, heat from the tropics is transported northward by the Kuroshio current, i.e., the western boundary current of the North Pacific subtropical gyre (Bryden and Imawaki 2001; Nagano et al. 2009, 2010). Excess heat is then released to the atmosphere in the Kuroshio Extension (KE) region, particularly in winter when cold dry wind from the Eurasian Continent blows over the warm KE. The KE region, for this reason, has been the subject of intensive research, e.g., the Kuroshio Extension System Study (KESS) (Donohue et al. 2008; Jayne et al. 2009; Konda et al. 2010) and long-term monitoring. In particular, in 2004 as a part of KESS, the Kuroshio Extension Observatory (KEO), a surface mooring on the southern side of the KE jet, was initiated to monitor and study the air–sea interaction associated with the large ocean surface heat loss. In 2007, the Japan Agency Marine-Earth Science and Technology (JAMSTEC) KEO (JKEO), a surface mooring, was initiated on the northern side of the KE jet. In this study, we use data from these moorings, in combination with hydrographic data from six research cruises and from Argo floats, to evaluate the water mass and in particular the salinity properties within the KE region.

Active air–sea interactions in the KE region generate various types of water masses, which are characterized by unique properties of temperature, salinity, and other parameters. As a result, the subsurface layer in the mid-latitude North Pacific is occupied by the North Pacific subtropical mode water (STMW) and central mode water (CMW) (Masuzawa 1972; Suga and Hanawa 1995; Suga et al. 1997; Oka and Qiu 2012). These water masses retain

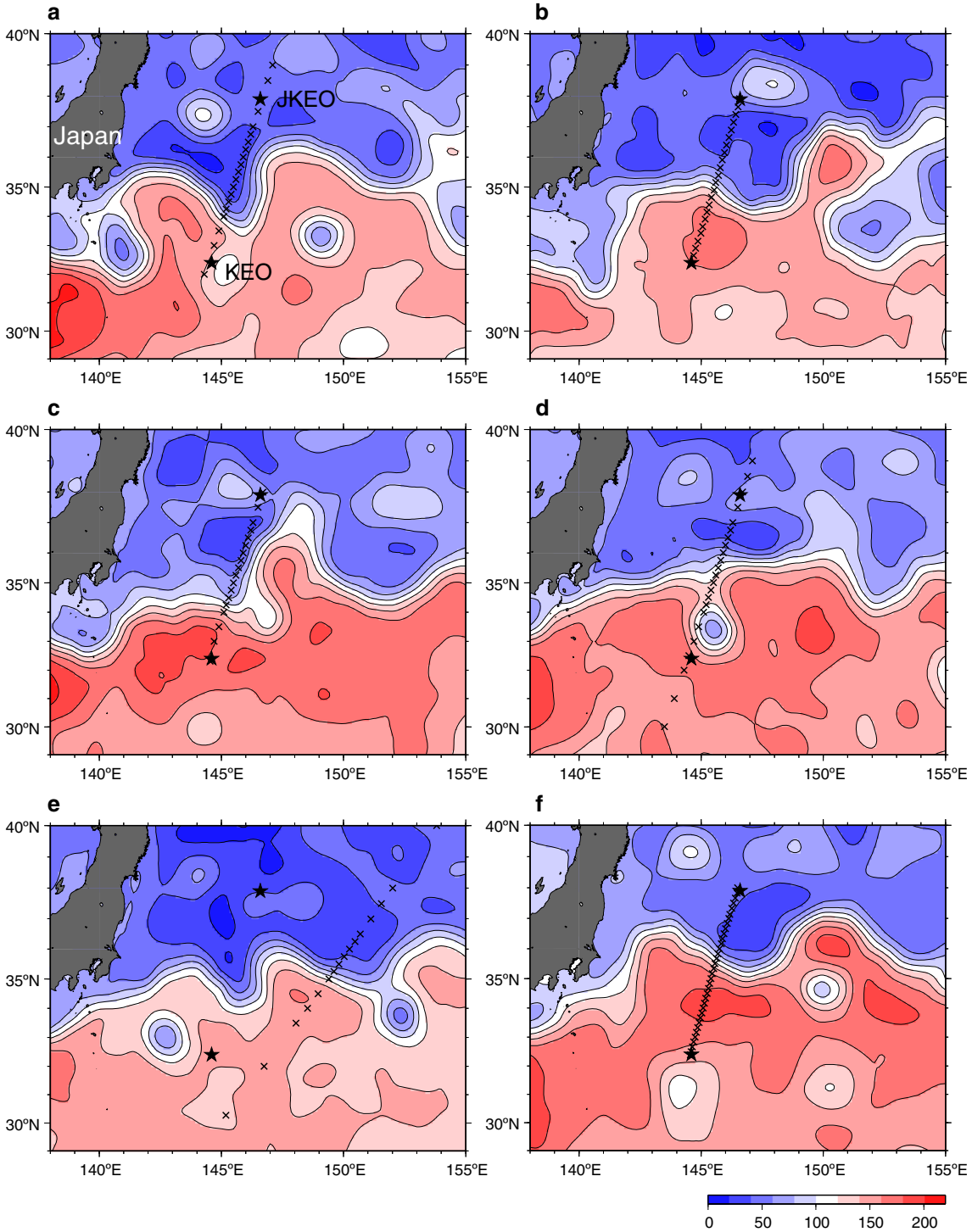


**Fig. 1** Locations of hydrographic stations (*crosses*) in **a** summer, **b** winter 2008, **c** summer, **d** autumn, **e** winter 2009, and **f** autumn 2010 cruises and KEO/JKEO buoy sites (*stars*) on absolute SSH maps in cm (*color shades*). Contour interval is 20 cm. SSH data were derived from Archiving, Validation and Interpretation of Satellite Oceanographic Data (AVISO)

a memory of the air–sea interactions during their formation in the KE region. When the mode waters reemerge in downstream regions, their sea surface temperature properties may be traced back to air–sea interactions from previous winters in the formation region, thus providing some predictability to the climate system (Alexander and Deser 1995). Sugimoto and Hanawa (2005) investigated where the STMW and CMW formation and reemergence

areas were located; Nagano et al. (2012a) examined their volume transport and impact on the heat transport of the subtropical gyre; and Rainville et al. (2014) mapped the STMW thickness and variability in the western North Pacific from 2002 to 2011.

Ocean and atmosphere variations in the KE region have been studied by many investigators (e.g., Vivier et al. 2002; Kelly 2004; Konda et al. 2010; Tomita et al. 2010; Cronin et al. 2013). Konda et al. (2010) showed how various types of cold-air outbreak weather patterns result in spatial patterns in latent and sensible heat loss with very large net surface heat loss on the warm side of the KE. Vivier et al. (2002), Kelly (2004), and Cronin et al. (2013) showed how, over long timescales, the heat loss by the ocean to the atmosphere is replaced by heat advected into the KE region. Based on data from the KEO mooring, Cronin et al. (2013) showed that vertical diffusive mixing across the bottom of the mixed layer can also be quite large in the southern KE region. As a result, summertime heating can precondition the winter mixed layer (Tomita et al. 2010). Nagano et al. (2013) estimated the volume transport of the Kuroshio south of Japan toward the KE region using a combination of hydrographic, inverted echo sounder, and satellite altimetric data. The Kuroshio in the East China Sea and the Ryukyu Current System east of the Ryukyu Islands are merged southeast of Kyushu (Nitani 1972; Nagano et al. 2009). Their combined volume transport is substantial, and its interannual variations can affect air–sea heat flux in the KE region (Nagano et al. 2013).

While many of these studies cited here focus on the heat balance and temperature distribution in the KE region, there has been less work on other properties of the water mass, e.g., salinity. Analysis of salinity variations can help distinguish different water masses and provides important information about the source of the water mass. For this reason, from 2008 to 2010, conductivity–temperature–depth (CTD) and expendable CTD (XCTD) hydrographic data were collected in the KE region. These data are used jointly with moored buoy observations at the KEO and JKEO stations on either side of the KE front (Fig. 1), and optimally interpolated Argo profiling float data are used here to analyze the origins of an anomalously high-salinity event in the winter mixed layer in the southern KE region. The data are described in Sect. 2, and the hydrographic features in the KE region are illustrated in Sect. 3. In Sect. 4, we discuss the origins of the salinity variations, and summarize our results in Sect. 5.

## 2 Observations and data

Hydrographic profiles down to depths over 1,000 m in the KE region were collected by the R/V *Kaiyo* and R/V *Mirai* of JAMSTEC using XCTD-1 (Tsurumi Seiki) and by the R/V *Syoyo-maru* of Fisheries Research Agency using a CTD SBE 911plus (Sea-Bird Electronics). Six sets of temperature and salinity data were obtained in summer (August 2008 and September 2009), autumn (November 2009 and November 2010), and winter (January 2009 and February 2010) (Table 1). The data obtained by the R/V *Kaiyo* and R/V *Mirai* are publicly available on JAMSTEC's Data Research System for Whole Cruise Information (DARWIN) (http://www.godac.jamstec.go.jp/darwin/e). The accuracies for the temperature and salinity XCTD data are 0.05 °C and 0.05 (psu), respectively, according to the estimations based on the differences between XCTD and CTD values by Mizuno and Watanabe (1998). In this paper, we vertically averaged profiles to reduce noisy features with vertical scales shorter than several meters and obtained profiles of potential temperature and salinity from 10 to 1,000 m at a vertical interval of 10 m.

National Oceanic and Atmospheric Administration (NOAA) and JAMSTEC started observations by moored buoys at stations KEO (32.4°N, 144.6°E) and JKEO (37.9°N, 146.6°E) from June 2004 and February 2007, respectively. For JKEO, temperature and salinity at depths from 1 to 500 m were measured by SBE 16 and SBE 37 (Sea-Bird Electronics); KEO temperature and salinity extended to ~525 m and were measured by NOAA Pacific Marine Environmental Laboratory (PMEL) temperature modules with Sea-Bird Electronic conductivity cells, and by SBE37, SBE39 and SBE51 sensors. All sensors were calibrated before the deployments and after the recoveries, and had accuracies better than 0.02 °C for temperature and 0.02 (psu) for salinity. Daily mean data were obtained from the project web sites for KEO (http://www.pmel.noaa.gov/OCS/KEO) and JKEO (http://www.jamstec.go.jp/iorgc/ocorp/ktsfg/data/jkeo). The daily averaged data were then averaged with a 1-month box-car filter to eliminate shorter timescale variations.

**Table 1** Research vessels, CTD/XCTD observation periods, and cruise names used in the present paper

| Year | Period | Cruise name |
|---|---|---|
| 2008 | | |
| R/V *Mirai* | Aug 1–3, 2008 | Summer 2008 |
| R/V *Syoyo-maru* | Jan 22–26, 2009 | Winter 2008 |
| 2009 | | |
| R/V *Kaiyo* | Sep 3–4, 2009 | Summer 2009 |
| R/V *Mirai* | Nov 5–7, 2009 | Autumn 2009 |
| R/V *Mirai* | Feb 11–13, 2010 | Winter 2009 |
| 2010 | | |
| R/V *Mirai* | Nov 5–6, 2010 | Autumn 2010 |

Grid point value of the monthly objective analysis using the Argo data (MOAA GPV) was compiled by Hosoda et al. (2008) and is maintained in the Japan Argo database (http://www.jamstec.go.jp/ARGO/argo_web/argo). The accuracies for temperature and salinity data collected by sensors on Argo floats are 0.005 °C and 0.01 (psu), respectively (Hosoda et al. 2008). Data collected by Argo floats, TRITON buoys, and ships from 2001 onward were optimally interpolated every month at the standard pressure levels with the horizontal grid interval of 1°. An increased number of hydrographic profiles have been deployed in the KE region since 2004, and the whole North Pacific since 2006, to examine the water mass variations. Therefore, we used the data from January 2004 to December 2010 for the analysis of the KE region and from January 2006 to December 2010 for the whole North Pacific region of 0–60°N, 120°E–100°W.

## 3 Results

Figure 2 shows sea surface dynamic height relative to the depth of 1,000 m or dbar on the observation lines with respect to the latitude relative to the KE current axis, defined by Kawai (1969, 1972) as an intersecting point of the 14 °C isotherm and the 200-m-depth level. Although sea surface dynamic height was occasionally disturbed by ubiquitous mesoscale eddies such as by a cyclonic eddy around 33°30′N, 145°30′E in November 2009 (hereafter called the autumn 2009 cruise as in Table 1) (Fig. 1d), all observations show the steep southward rise of the dynamic height characteristic of the KE current axis (Fig. 2), and altimetry shows that the maximal and minimal SSH on either end are located in the southern anticyclonic and northern cyclonic recirculations (Howe et al. 2009; Jayne et al. 2009). While the maximal and minimal dynamic height points in the winter 2009 observation (Fig. 1e) are 2°–5° of longitude apart from the locations of the maximal and minimal dynamic height points in the other observations, they are representative of the interior regions of the southern and northern recirculation gyres, respectively. The main pycnocline in the southern recirculation also shows large variability, being shallow ∼400 m in summer 2008 (red inverted triangle in Fig. 3a) and deep ∼500 m in winter 2009 (Fig. 3e).

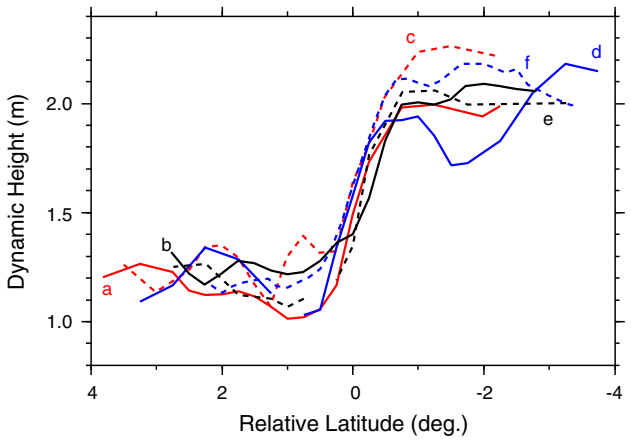


**Fig. 2** Sea surface dynamic height with respect to relative latitude from the current axis of the KE during cruises in **a** August 2008, **b** January 2009, **c** September 2009, **d** November 2009, **e** February 2010, and **f** November 2010. The reference level was set to the depth of 1,000 dbar for (**b**), i.e, the winter 2008 cruise, and 1,000 m for the other cruises. Summer, autumn, and winter sections are *red*, *blue* and *black*, respectively

Sections of potential temperature and salinity are shown in Figs. 4 and 5, respectively. Associated with the strongly baroclinic KE, the potential temperature and salinity of the main pycnocline shoals sharply to the north. In the summer 2008 and 2009 observations, the seasonal thermocline extends from the base of the surface mixed layer down to a depth of approximately 100 m, and is apart from and in contact with the main thermocline in the southern and northern sides of the KE, respectively (Fig. 4a, c). Due to the existence of the seasonal thermocline, the salinity maximum water in the underlying layer is insulated from the sea surface low-salinity water (Fig. 5a, c). The subsurface saline water in the southern KE region is much saltier than that in the northern region, being mainly derived from the North Pacific tropical water (TW) (Taft 1978) formed by the excessive evaporation over precipitation in the central North Pacific (Suga et al. 2000). In the winter cruises, a vertically uniform potential temperature layer (i.e., a deep surface mixed layer) develops (Fig. 4b, e) and takes up the subsurface water. As a result, during winter, the water in the mixed layer is saltier (Fig. 5b, e) than in other seasons.

Such seasonal variations are particularly noticeable around the maximal and minimal dynamic heights in the southern (Figs. 4, 5, red inverted triangles) and northern (blue inverted triangles) recirculation gyres. To view the mixed layer in more detail, potential temperature profiles in the recirculations observed during the winter and summer cruises (Table 1) are shown in Fig. 6. Following de Boyer Montégut et al. (2004), we defined the bottom of the winter mixed layer as the depth where potential temperature is 0.2 °C lower than that at the uppermost 10 m depth. Associated with the intensification of the southern recirculation in winter 2009 as indicated in Fig. 3e, the winter mixed layer (black dashed line in Fig. 6a) reached to a depth of 310 m, which is approximately twice as deep as the 160 m depth found in winter 2008 (black solid line) and is deeper than the climatological mixed layer depth (e.g., see the winter mixed layer depth map in fig. 5 of

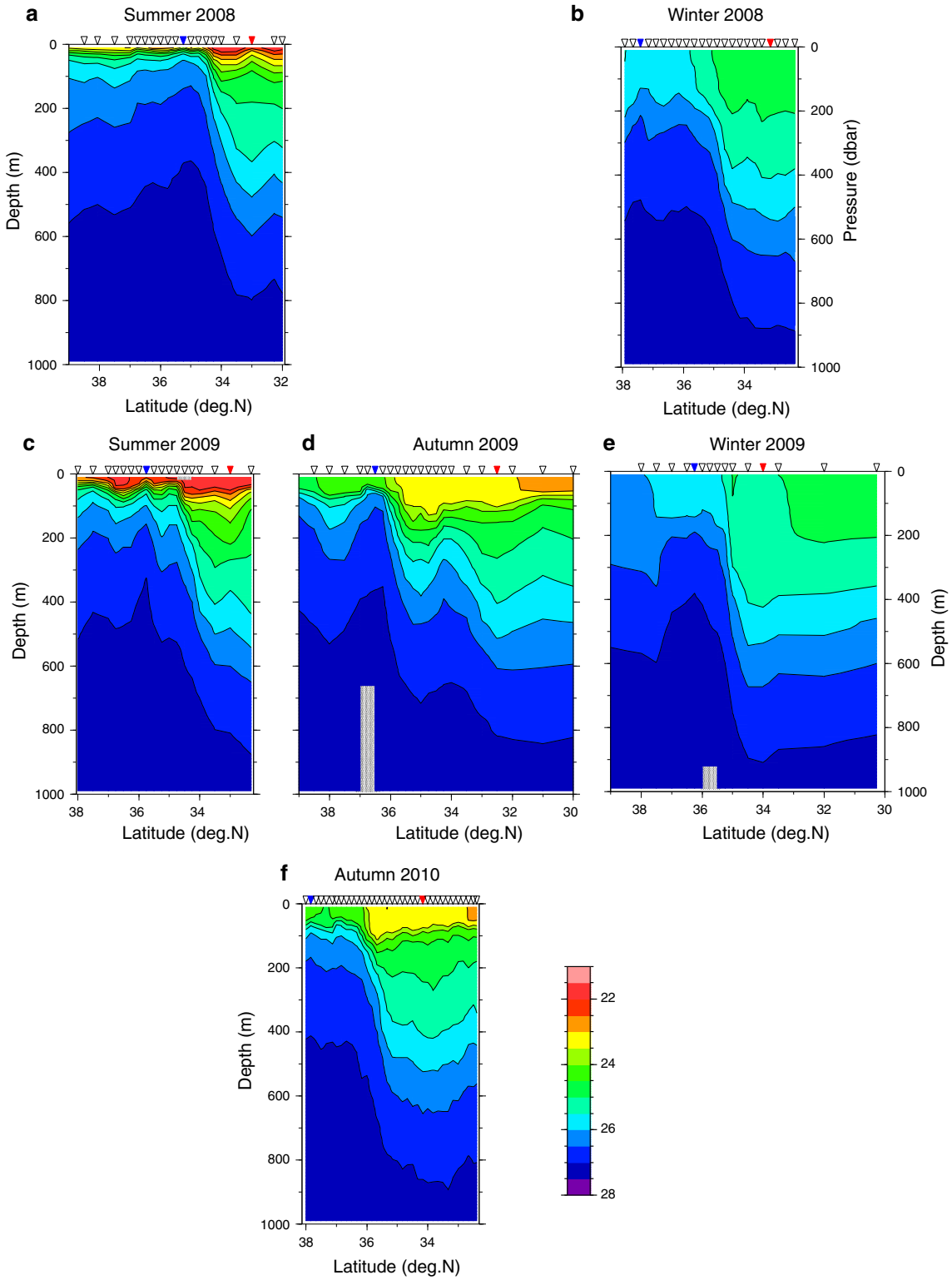


**Fig. 3** Sections of potential density, $\sigma_\theta$, (kg m$^{-3}$) in **a** August 2008, **b** January 2009, **c** September 2009, **d** November 2009, **e** February 2010, and **f** November 2010. Contour interval is 0.5 kg m$^{-3}$, and *color bar* is indicated to the *right* of **f**. *Gray shading* indicates no data, and *inverted triangles* at the *top* of the *panels* represent the hydrographic points. *Red* and *blue triangles* show the sites of the maximal and minimal sea surface dynamic heights, respectively

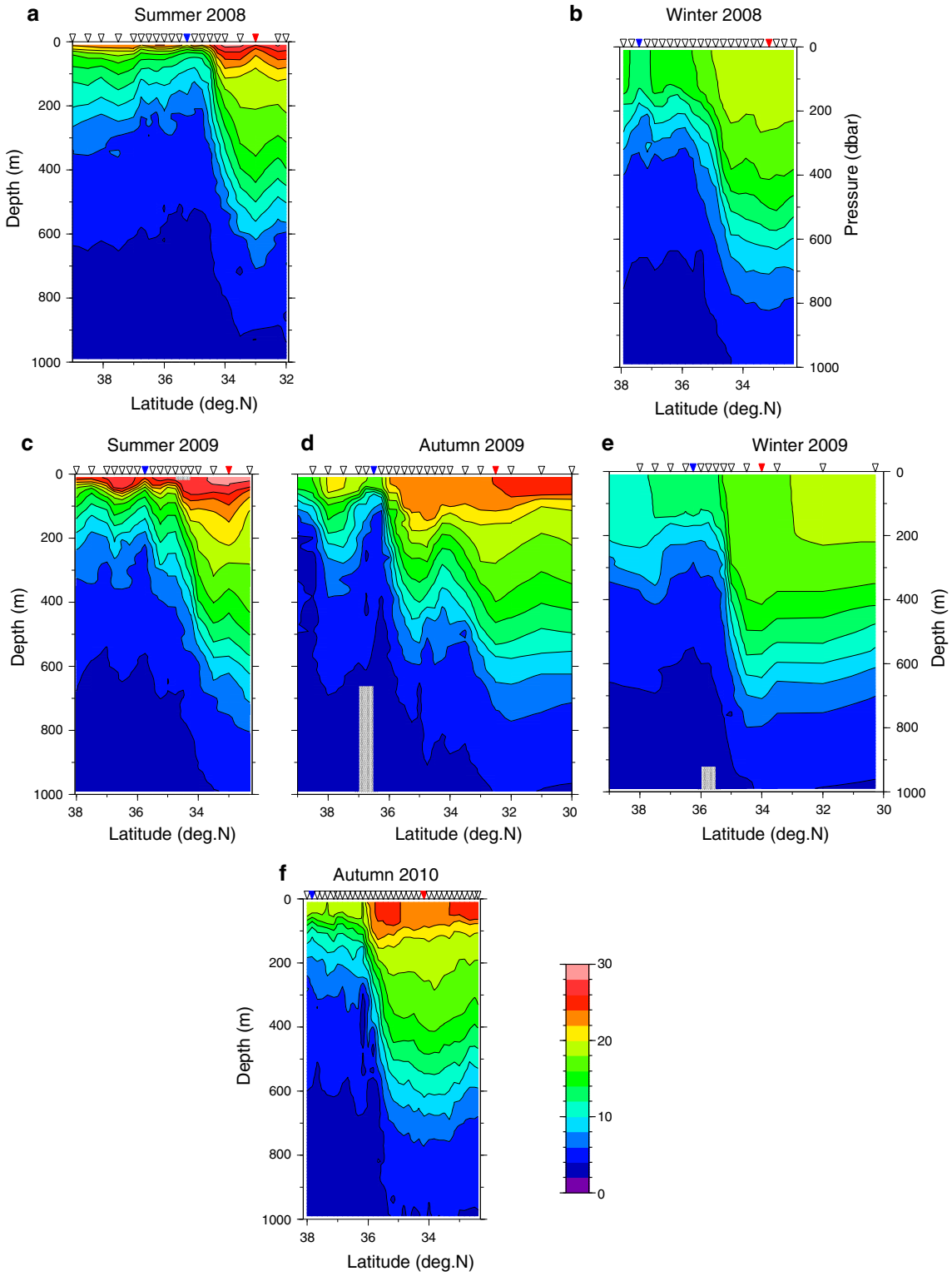


**Fig. 4** Same as Fig. 3, but for potential temperature (°C). Contour interval is 2 °C

de Boyer Montégut et al. 2004). In the northern recirculation, the winter mixed layer was significantly shallower and relatively less variable, being 90 and 140 m depths in winters 2008 and 2009, respectively (Fig. 6b). Clearly, the southern recirculation winter mixed layer depth varies substantially on interannual timescales.

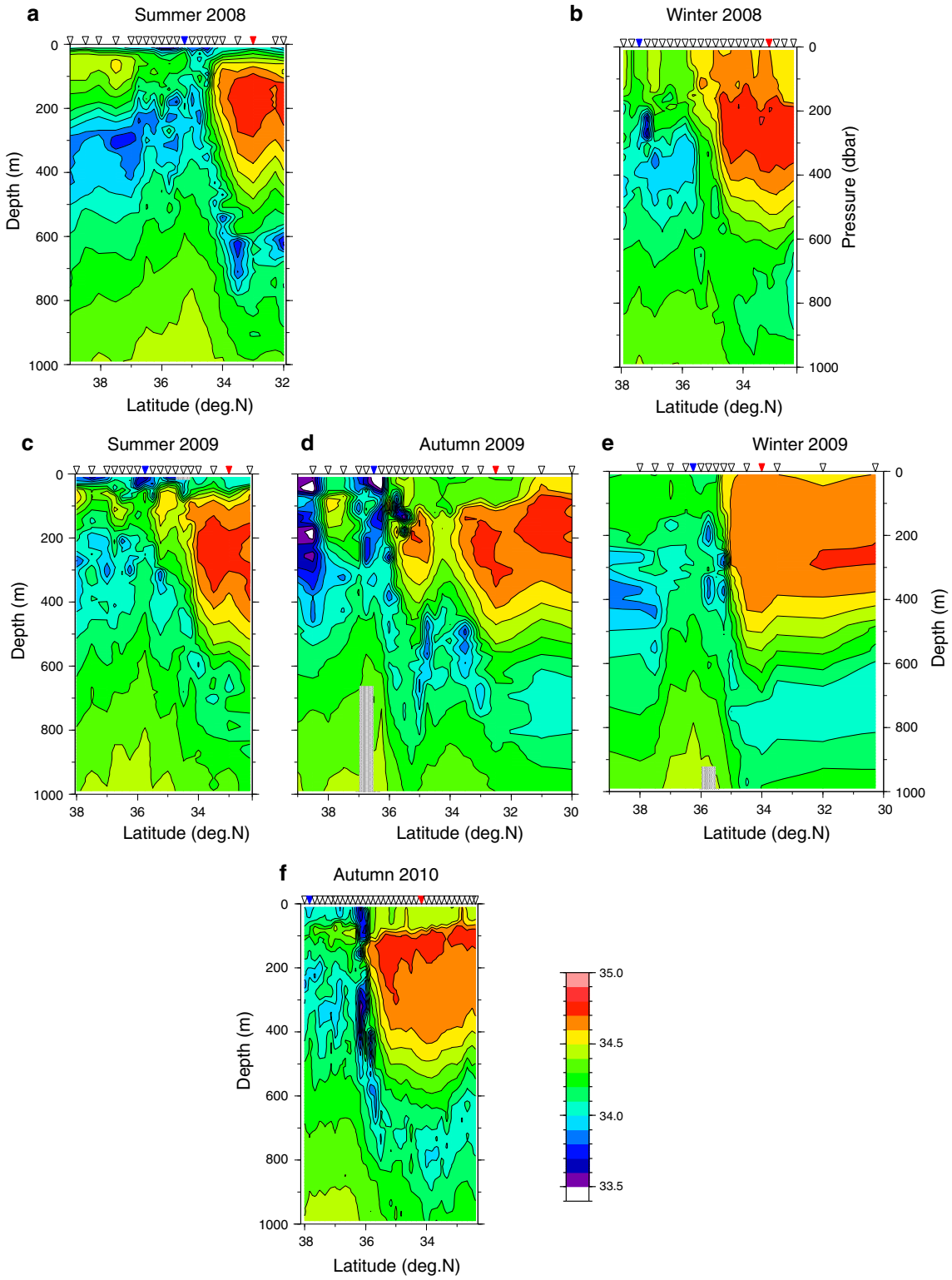


**Fig. 5** Same as Fig. 3, but for salinity. Contour interval is 0.1 (psu)

Salinity profiles are shown in Fig. 7. If near-surface water is not advected and freshwater is not injected or depleted from the sea surface, winter near-surface salinity ($S_W$) should be equivalent to the vertically averaged value of summer salinity profile ($S_S$), i.e., $S_W = \overline{S_S}$, where

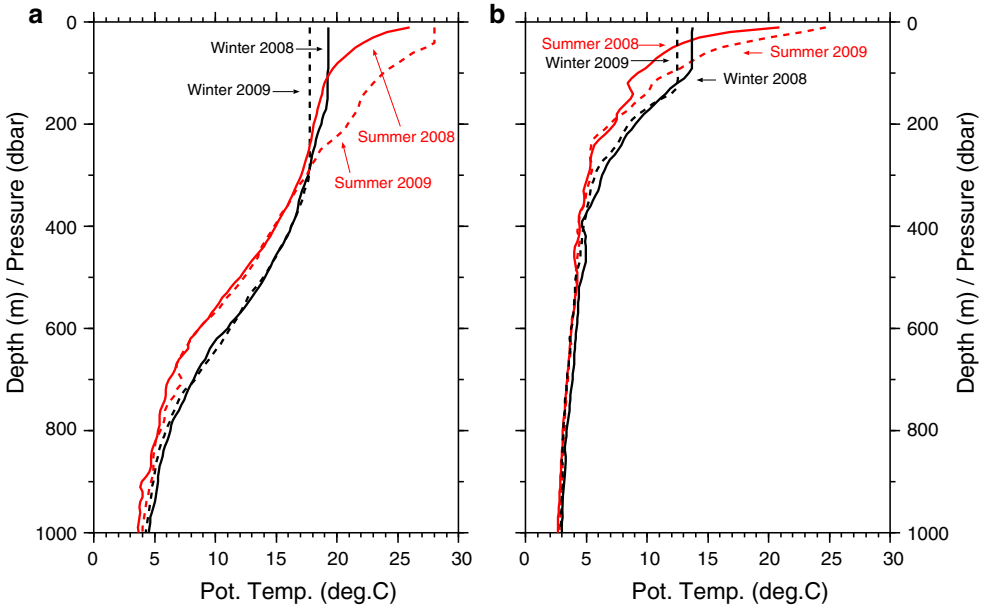


**Fig. 6** Potential temperature profiles at the **a** maximal and **b** minimal sea surface dynamic heights in summer cruises in 2008 (*red solid line*) and 2009 (*red dashed line*); and winter cruises in 2008 (*black solid line*) and 2009 (*black dashed line*). Locations of the maximal and minimal sea surface dynamic heights are indicated by *red* and *blue inverted triangles* at the *top* of *panels* in Fig. 4, respectively

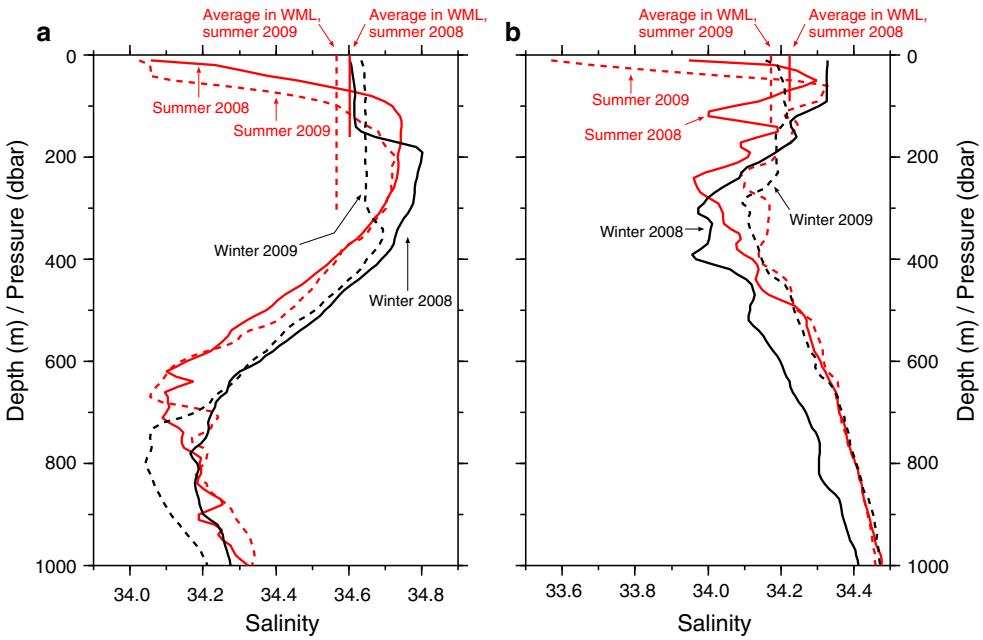


**Fig. 7** Same as Fig. 6, but for salinity. Salinity in summer 2008 and 2009 cruises averaged from the sea surface to the bottom depth of the following winter mixed layer, i.e., $\overline{S_S}$ in Eq. (1), are illustrated by *vertical red solid* and *dashed lines*, respectively

$$\overline{S_S} = \frac{1}{D_W} \int_{-D_W}^{0} S_S(z)\,dz. \quad (1)$$

Here, $z$ is the vertical coordinate and $D_W$ is the winter mixed layer depth. Otherwise, $S_W \neq \overline{S_S}$. The average salinity value in the southern recirculation in summer 2008 (Fig. 7a, red vertical solid line) is nearly equivalent to salinity in the winter mixed layer in following winter 2008 (January 2009) (black solid line); the salinity value in the winter cruise could thus be explained by one-dimensional vertical diffusive mixing, consistent with the Cronin et al. (2013) analysis of the development of the deep mixed layer at KEO in late 2004.

Meanwhile, the average salinity value in summer 2009, 34.57 (red vertical dashed line), is significantly smaller than 34.65 in the anomalously deep mixed layer in the following winter 2009 (black dashed line); i.e., $S_W \neq \overline{S_S}$. The increase of salinity in the anomalously deep mixed layer in the southern recirculation in winter 2009 might be attributable to the horizontal advection of saltier water in addition to the local evaporative freshwater loss to the

atmosphere. Note that the excessive amount of salinity content in the mixed layer in winter 2009 relative to that in the summer integrated down to the bottom of the winter mixed layer is 24.5 psu m, which is an order of magnitude larger than 2.6 psu m in 2008. In the northern recirculation (Fig. 7b), salinity content moderately increased by 9.2 and 4.9 psu m from summer to winter in 2008 and 2009, respectively.

By using freshwater flux, i.e., evaporation minus precipitation, based on the data of National Centers for Environmental Prediction/National Center for Atmospheric Research (Kistler et al. 2001), we calculated year-to-year variation of the freshwater flux in the southern KE region. As a result, upward freshwater flux was found to decrease from winter 2008 to winter 2009 by approximately 0.4 mm day$^{-1}$. In addition, because salinity decreases with the depth beneath the bottom of the mixed layer (Fig. 7a), entrainment from the underlying layer could not account for the salinity increase in the mixed layer in winter 2009.

In addition, near-surface salinity in the southern KE region generally decreases eastward, as, for example, Oka (2009) illustrated in the STMW layer. Because the winter 2009 cruise line is located approximately a few hundred kilometers east from (Fig. 1c, e) and in fresher near-surface background water than the summer 2009 cruise line, the high-salinity anomaly observed in winter 2009 is not attributable to the eastward displacement of the observation line. Thus, advection appears to be the primary contributor to the year-to-year variation of salinity in the southern KE region. This hypothesis is evaluated in more detail in Sect. 4.

Since the KEO and JKEO buoys were located within the southern and northern recirculation gyres, respectively, their data can provide partial information about the variations in the near-surface temperature and salinity (Fig. 8a, b). In particular, anomalously low salinity is seen at KEO in 2006 and anomalously low temperature is seen at JKEO in late 2009. Seasonal variations in sea surface temperature are larger at JKEO than at KEO. KEO wintertime sea surface salinity values are generally high. At JKEO, spiky decreases of salinity below 33.5 (psu) were observed frequently such as in August 2008 and April and July 2009 (Fig. 8b). The anomalously low-salinity water marked *a* in Fig. 8b was not detected by the ship observation in the summer 2008 cruise (Fig. 5a). Meanwhile, patchy anomalously low-salinity water masses in the surface layer at a few sites to the north of 36°N and 38°N were observed during the autumn 2009 cruise (Fig. 5d), but were not observed by the buoy at JKEO in the period marked *d* in Fig. 8b. The spatial scales of the low-salinity water masses in the northern KE region are too small to be detected commonly by both buoy and ship observations. Such a

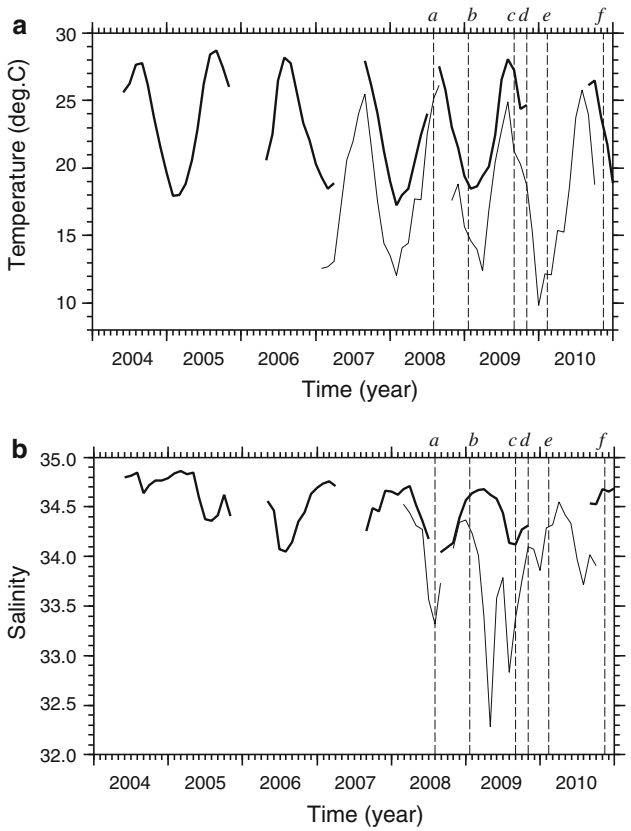


**Fig. 8** Monthly **a** temperature and **b** salinity at 1 m depth at KEO (*thick solid line*) and JKEO (*thin solid line*). *Vertical dashed lines* and *letters above* them indicate the periods of the hydrographic observations by research vessels

low-salinity water mass has been reported to be present in the region southeast of Hokkaido and east of Tohoku, i.e., the Oyashio region, (Kawai 1972) and transported to the KE region by mesoscale or smaller eddies (Okuda et al. 2001). The small-scale low-salinity water masses observed in northern KE region appear to be associated with eddies advected from the Oyashio region.

Because the buoy data have occasional gaps, owing for example to mooring line breaks such as in April 2007 at KEO and in September 2008 at JKEO, it is not possible to fully resolve seasonal versus interannual variations in these data. Instead, the optimally interpolated Argo float data are used to examine the interannual variations of temperature and salinity in the KE region. We show interannual variations of near-surface (10 dbar) temperature and salinity after removing the mean seasonal variations at KEO and JKEO based on the MOAA GPV data in Fig. 9; smoothing was performed with a 5-month box-car filter to remove high-frequency mesoscale fluctuations. Low salinity in the southern KE region in 2006 and anomalously low temperature in the northern region in 2009, seen in the buoy data (Fig. 8), can also be seen in the MOAA GPV data, as

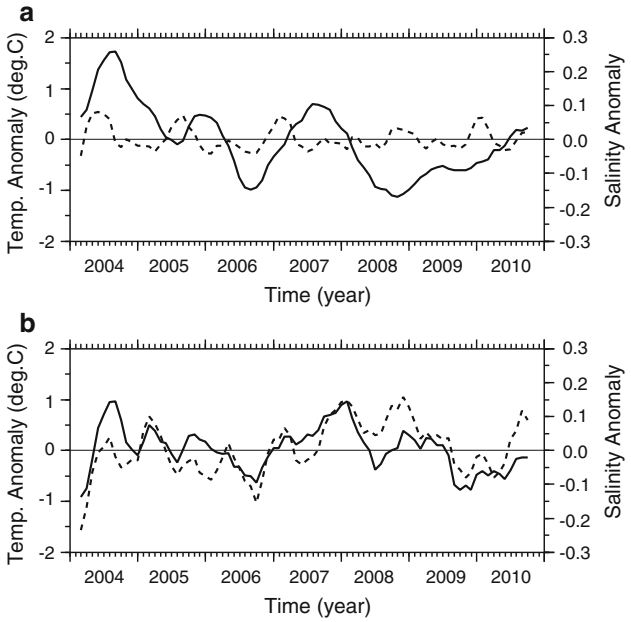


**Fig. 9** Interannual variations of temperature (*dotted lines*) and salinity (*solid lines*) in **a** southern and **b** northern KE regions at 10 dbar from 2004 to 2010. Data are based on MOAA GPV data

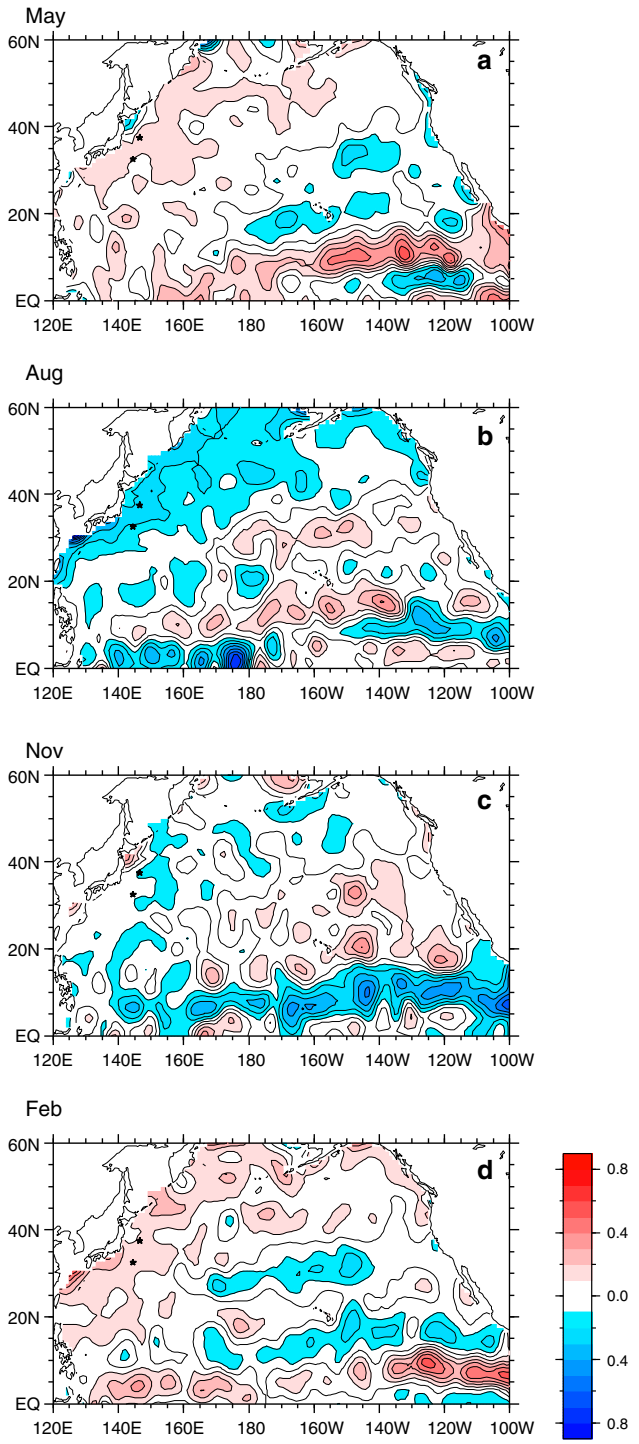


**Fig. 10** Mean seasonal anomaly of salinity at 10 dbar in **a** May (spring), **b** August (summer), **c** November (autumn), and **d** February (winter). Contour interval is 0.1. Locations of the KEO and JKEO sites are indicated by *stars*

shown in Fig. 9. In other words, temperature and salinity in the southern (KEO) and northern (JKEO) KE regions vary on interannual timescales.

In the southern KE region (Fig. 9a), salinity fluctuates independently of temperature with a low correlation coefficient of 0.13. Notably, salinity increased from November 2008 to September 2010 (Fig. 9a), consistent with the high-salinity anomaly in the southern recirculation observed during the winter 2009 cruise (Figs. 1e, 5e, 7a). Peaks in the mid-2004, late 2005, and mid-2007 (Fig. 9a) suggest that, on these occasions, more saline water might be supplied to the southern KE region, although synoptic hydrographic sections are not available. Meanwhile, in the northern KE region (Fig. 9b), the variations of temperature and salinity are related to each other with a correlation coefficient of 0.61, which is higher than the 99 % significance level (0.56) based on the Student's *t*-test. Both temperature and salinity time series at JKEO have large peaks at an interval of approximately 4 years such as in 2005 (2004) and 2008 (2008) for temperature (salinity).

## 4 Discussion

In this section, we discuss the origins of the salinity anomaly in the KE region, expanding the study region to the whole North Pacific. We show the mean seasonal anomaly of salinity from spring (Fig. 10a) to winter (Fig. 10d) at the level of 10 dbar. Both KEO and JKEO sites are located in the region of a substantial seasonal variation, which is attributable to the seasonal variation of local evaporation minus precipitation (Bingham et al. 2012) and to the uptake of the deep high-salinity water to

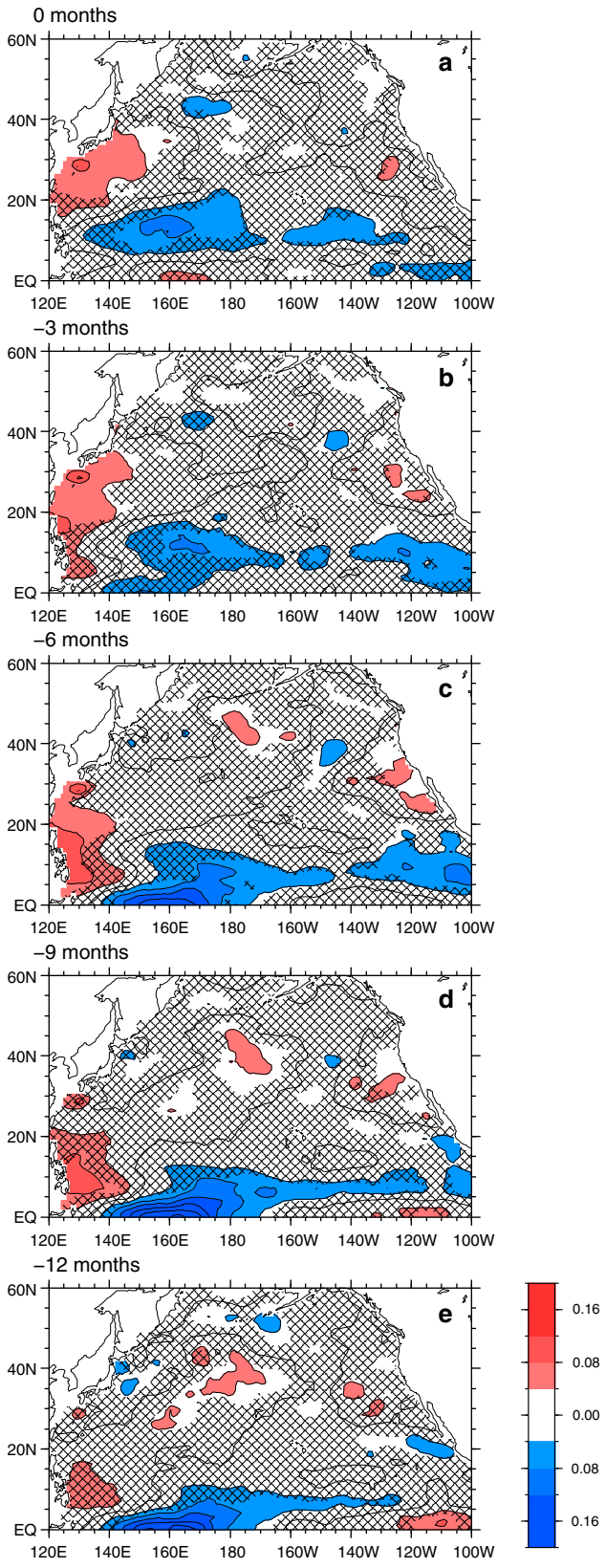


◀**Fig. 11** Time lead covariance of the interannual salinity variation at 10 dbar relative to KEO site, i.e., $C_\tau$(KEO) in Eq. (2). Time lead, $\tau$, is taken every 3 months from **a** 0 to **e** 12 months. Contour interval is 0.04, and *color bar* is indicated to the *lower right*. *Hatching* shows regions with correlations lower than the 95 % significance level. Calculations were performed by using data from 2006 to 2010

the winter mixed layer as described in Sect. 3. Greater seasonal salinity variations are present in the intertropical convergence zone (ITCZ) in the equatorial and tropical North Pacific regions, but do not migrate toward the KE region. Thus, the seasonal salinity variation at the KE region is forced locally.

Next, we discuss the interannual salinity variations in the whole North Pacific. Salinity would be conserved following a water parcel if it moves without significant addition and removal of freshwater. On the basis of this idea, we trace the variation of salinity with respect to the variations at KEO and JKEO by applying a covariance method to the salinity anomaly data of MOAA GPV from 2006 to 2010. We express salinity at time $t$ and location $\boldsymbol{x}$ as $S_t(\boldsymbol{x})$, and covariance relative to $\boldsymbol{x}_\mathrm{r}$ with time lead $\tau$ as $C_\tau(\boldsymbol{x},\boldsymbol{x}_\mathrm{r})$. The time lead covariance is defined as

$$C_{m\Delta t}(\boldsymbol{x},\boldsymbol{x}_\mathrm{r}) = \sum_{n=m}^{N}[S_{(n-m)\Delta t}(\boldsymbol{x}) - \overline{S}(\boldsymbol{x})][S_{n\Delta t}(\boldsymbol{x}_\mathrm{r}) - \overline{S}(\boldsymbol{x}_\mathrm{r})]/(N-m), \quad (2)$$

where $\Delta t$ is the temporal interval of the data, $m$ is the number of the temporal lead interval, $N$ is the number of data averaged in the covariance, and overbar indicates time-averaging. This technique is useful for revealing the spatiotemporal characteristics of the salinity covariations. In this study, $\boldsymbol{x}_\mathrm{r}$ was set to the locations of the KEO and JKEO sites, and $\tau = m\Delta t$ was taken up to 12 months.

Simultaneous covariance of salinity relative to that at KEO, i.e., $C_0$(KEO), (Fig. 11a) shows a significant peak in the region southeast to south of Japan, exceeding 0.04. With the time leads of 3–9 months, the covariance peak moves southward along the western subtropical North Pacific and becomes higher, leading 3 months in advance near the Ryukyu Islands around 25°N, 130°E (Fig. 11b), 6 months in advance near the eastern region of Taiwan (Fig. 11c), and 9 months in advance near the Philippines (Fig. 11d). The covariance in the Philippine Sea is insignificant at the time lead of 12 months (Fig. 11e). The attenuating propagation of the covariance peak along the western regions suggests that the high-salinity anomaly was advected from the region off the east coast of the Philippines to the southern KE region but was affected by sea surface freshwater flux variation such as local freshening due to excessive rainfall found by Sugimoto et al. (2013).

In Fig. 12, we show a Hovmöller diagram of the salinity anomaly variation at 10 dbar along the western branch of the subtropical gyre. Positive salinity anomalies were

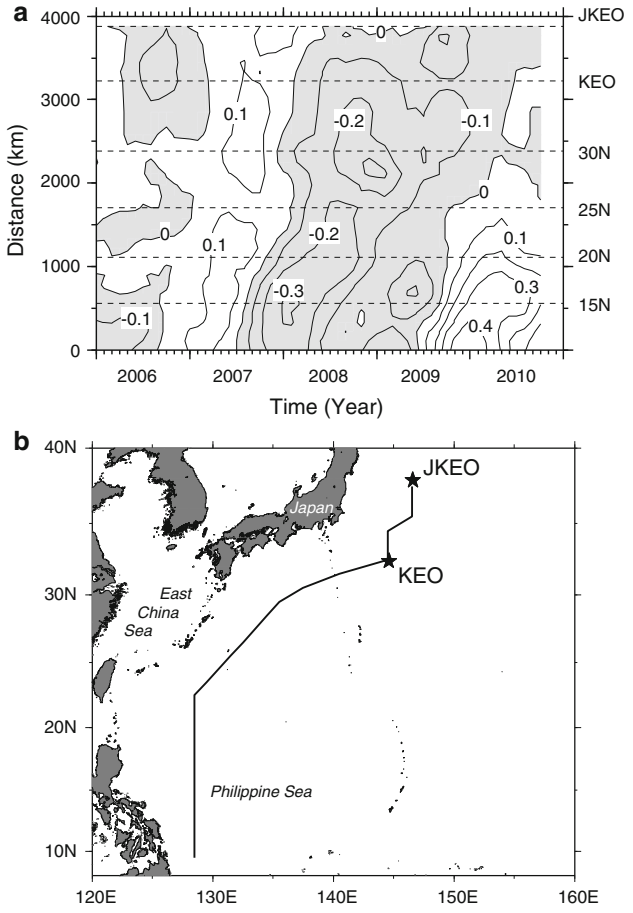


**Fig. 12** **a** Hovmöller diagram of the salinity anomaly variation at 10 dbar along the western branch of the subtropical gyre for the period from 2006 to 2010. The diagram was plotted along the line from the Philippine Sea to JKEO via KEO (*stars*) as shown by the *line* in (**b**). Ordinate in (**a**) is distance along the line from the southern end, and *horizontal dashed lines* indicate latitudes of 15°N, 20°N, 25°N, 30°N, KEO, and JKEO. *Shading* indicates negative anomalies, and contour interval is 0.1

generated in association with the El Niño of 2006/2007 and 2009/2010, and propagate from the Philippine Sea to the southern KE region. Sea surface freshwater forcing and current pattern in the tropical region are known to have large variations associated with El Niño. During El Niño, precipitation in the Philippine Sea is significantly reduced (Dai and Wigley 2000), and the bifurcation latitude of the North Equatorial Current (NEC) migrates northward to the east of the Philippines (e.g., Qiu and Chen 2010), possibly reducing the amount of low-salinity water under the ITCZ that gets fed into the southern border of the Kuroshio. Their combined effect may thus increase the salinity of the near-surface water proceeding to the KE region. The northward migration of the salinity anomalies to the southern KE region is notably slower than the midlatitude atmospheric responses to El Niño such as studied by Horel and Wallace (1981) and others, so that the northward migration seems not to be attributable to the forcing by the atmospheric teleconnections. Other processes occurring during the poleward transit may also play a role. For example, as shown in Fig. 12, the large positive anomaly in 2009/2010 was rapidly attenuated during the poleward transit, whereas the small positive anomaly in 2006/2007 was relatively unchanged.

The average advection speed of the salinity variation was estimated to be approximately 17 cm $s^{-1}$, which is much smaller than the current speed around the Kuroshio current axis in the East China Sea (e.g., see the mean current velocity section in fig. 7a of Andres et al. 2008) but is similar to that of the near-surface northeastward current east of the Ryukyu Islands based on the current measurements by a lowered acoustic Doppler current profiler (see the velocity profiles in fig. 2a of Nagano et al. 2012b). The decorrelation radius of the MOAA GPV data ($\sim$1,000 km) is so large that the MOAA GPV gridded salinity variation in the western branch of the subtropical gyre includes variations from the East China Sea Kuroshio, the northeastward current east of the Ryukyu Islands, and the interior southwestward return current. However, because the concentration of the Argo floats in the East China Sea is rather low, the signal of the salinity variation migrating toward the southern KE region based on MOAA GPV data appears to be affected predominantly by the salinity variation in the near-surface northeastward flow east of the Ryukyu Islands and Taiwan.

A salinity variation, inversely related to that in the southern KE region, was found in the region of 10°N–15°N, 150°E–160°W, with a negative covariance below −0.04 (Fig. 11a). This inverse covariation can be traced back 9 months to the western equatorial region between 140°E and 180° (Fig. 11d). Unlike the interannual variation of salinity proceeding to the southern KE region, the inverse variation of salinity does not migrate to the north of approximately 20°N in the interior region where south- or southwestward return currents prevail.

The covariance of the salinity variation relative to that at JKEO with no time lead, i.e., $C_0$(JKEO), (Fig. 13a) is distinctly positive in the eastern region of Japan and the western equatorial region between 140°E and 180°, whereas that in the eastern region of the Philippines is negative. With the time leads up to 12 months (Fig. 13b–e), the covariance in the eastern region of Japan is diminished and is traced back neither to the Philippine Sea nor to the subarctic regions. Accordingly, the salinity variation in the northern KE region is not principally attributed to the horizontal advection of the salinity variation. Because the winter mixed layer in the northern KE region is relatively shallow (Fig. 6b), local evaporative freshwater loss and

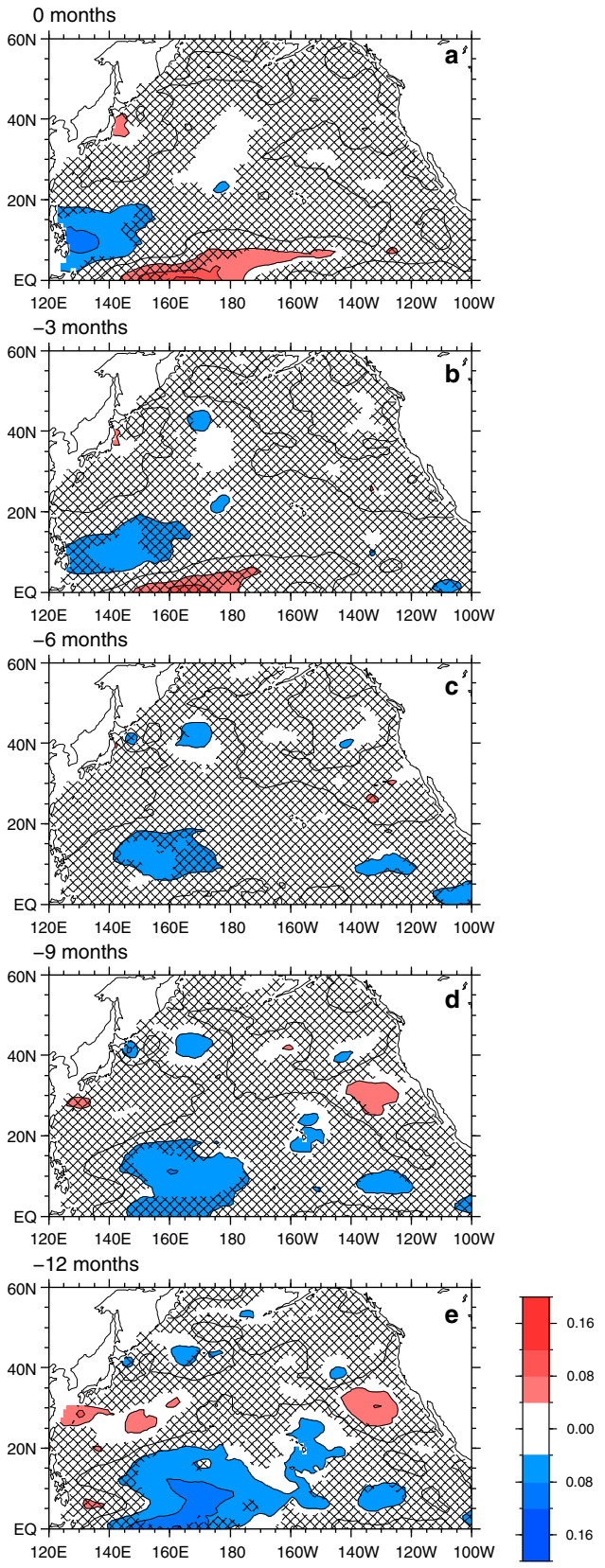


**Fig. 13** Same as Fig. 11, but for JKEO site, i.e., $C_\tau$(JKEO) in Eq. (2)

mixing likely affect the near-surface salinity variation in the northern KE region more strongly than that in the southern region.

## 5 Summary and conclusion

We examined hydrographic features in the KE region using the data collected by six research cruises. In summer, the seasonal thermocline insulates the near-surface low-salinity water from the underlying high-salinity water. Salinity in the subsurface layer is much higher in the southern KE region than that in the northern region because the southern water is mainly derived from the TW. In winter, the mixed layer develops and takes up the subsurface high-salinity water; as a result, near-surface water becomes saltier and colder than in other seasons. Moreover, we found a very large year-to-year hydrographic change: the salinity in the anomalously deep winter mixed layer in the February 2010 exceeded the salinity from the previous summer (September 2009).

Using optimally interpolated Argo float data, we investigated the source of the excessive salinity in the 2009 winter near-surface layer. The interannual variation of salinity in the southern KE region is independent of temperature. The origin of the salinity variation was traced back to the region off the east coast of the Philippines. In other words, the horizontal advection of the interannual salinity variation from the Philippine Sea cannot be ignored in the water mass variation in the southern KE region. The water mass is modified in the Philippine Sea, presumably due to precipitation variations in the western tropical North Pacific and equatorial regions by El Niño, and is transported along the western subtropical North Pacific by northeastward current with an elapsed time of approximately 9 months, giving an average advection speed of approximately 17 cm $s^{-1}$. Meanwhile, salinity and temperature covary in the northern KE region on timescales of approximately 4 years, presumably due to local mixing and surface processes.

The results of the present study provide information about the life history of the water mass occupying the near-surface layer in the KE region. Past studies on the properties of the water masses interacting with, or reemerging to interact with the atmosphere in the Kuroshio and KE regions have generally focused on local or regional ventilation processes and have not taken into account water masses that are remotely generated in the tropics east of the Philippines. Further work is needed to understand how the high-salinity anomaly is generated in the Philippine Sea by El Niño events and the relationship between water mass variations in the Philippine Sea and ocean–atmosphere

interaction in the mid-latitude North Pacific. Long-term monitoring of hydrographic variations in both key areas, i.e., the KE region and Philippine Sea, may provide us a new insight into the mid-latitude ocean–atmosphere interaction.

**Acknowledgments** The authors thank the captains, crew, technicians, and scientists for collecting ship data on board the R/V *Kaiyo*, R/V *Mirai*, and R/V *Syoyo-maru* (cruise numbers: MR08-03, MR09-04, MR10-01 leg 2, MR10-06, KY09-07, and SY08-04), for the observations by KEO and K-TRITON (JKEO) buoy systems, and for special efforts by Drs. K. Matsumoto, M. Honda, and Y. Kashino. The authors also thank Drs. M. Konda, S. Hosoda, and T. Hasegawa for their helpful comments. Thanks are extended to anonymous reviewers for their helpful comments. This work was partly supported by the Ministry of Education, Culture, Sports, Science and Technology (MEXT), Grant-in-Aid for Scientific Research on Innovative Areas (22106007).

## References

Alexander MA, Deser C (1995) A mechanism for the recurrence of wintertime midlatitude SST anomalies. J Phys Oceanogr 25:122–137

Andres M, Wimbush M, Park J-H, Chang K-I, Lim B-H, Watts DR, Ichikawa H, Teague WJ (2008) Observations of Kuroshio flow variations in the East China Sea. J Geophys Res 113(C05013). doi:10.1029/2007JC004200

Bingham FM, Foltz GR, McPhaden MJ (2012) Characteristics of the seasonal cycle of surface layer salinity in the global ocean. Ocean Sci 8:915–929. doi:10.5194/os-8-915-2012

Bryden H, Imawaki S (2001) Ocean heat transport. In: Siedler H, Church J, Gould J (eds) Ocean circulation and climate: observing and modeling the global ocean. Academic, London, pp 455–474

Cronin MF et al (2013) Formation and erosion of the seasonal thermocline in the Kuroshio Extension Recirculation Gyre. Deep Sea Res II 85:62–74. doi:10.1016/j.dsr2.2012.07.018

Dai A, Wigley TML (2000) Global patterns of ENSO-induced precipitation. Geophys Res Lett 27(9):1283–1286. doi:10.1029/1999GL011140

de Boyer Montégut C, Madec G, Fischer AS, Lazar A, Iudicone D(2004) Mixed layer depth over the global ocean: an examination of profile data and a profile-based climatology. J Geophys Res 109(C12003). doi:10.1029/2004JC002378

Donohue K et al (2008) Program studies the Kuroshio Extension. EOS Trans AGU 89(17):161–162. doi:10.1029/2008EO170002

Horel JD, Wallace JM (1981) Planetary-scale atmospheric phenomena associated with the southern oscillation. Mon Weather Rev 109:813–829

Hosoda S, Ohira T, Nakamura T (2008) A monthly mean dataset of global oceanic temperature and salinity derived from Argo float observations. JAMSTEC Rep Res Dev 8:47–59

Howe PJ, Donohue KA, Watts R (2009) Stream-coordinate structure and variability of the Kuroshio Extension. Deep Sea Res I 56:1093–1116. doi:10.1016/j.dsr.2009.03.007

Jayne SR et al (2009) The Kuroshio Extension and its recirculation gyres. Deep Sea Res I 56:2088–2099. doi:10.1016/j.dsr.2009.08.006

Kawai H (1969) Statistical estimation of isotherms indicative of the Kuroshio axis. Deep Sea Res Suppl. 16:109–115

Kawai H (1972) Hydrography of the Kuroshio Extension. In: Stommel H, Yoshida K (eds) Kuroshio—its physical aspects. University of Tokyo Press, Tokyo, pp 235–352

Kelly KA (2004) The relationship between oceanic heat transport and surface fluxes in the western North Pacific: 1970–2000. J Clim 17:573–588

Kistler R et al (2001) The NCEP-NCAR 50-year reanalysis: monthly means CD-ROM and documentation. Bull Am Meteorol Soc 82:247–267

Konda M, Ichikawa H, Tomita H, Cronin MF (2010) Surface heat flux variations across the Kuroshio Extension as observed by surface flux buoys. J Clim 23(19):5206–5221. doi:10.1175/2010JCLI3391.1

Masuzawa J (1972) Water characteristics of North Pacific central region. In: Stommel H, Yoshida K (eds) Kuroshio—its physical aspects. University of Tokyo Press, Tokyo, pp 95–127

Mizuno K, Watanabe T (1998) Preliminary results of in-situ XCTD/CTD comparison test. J Oceanogr 54:373–380

Nagano A, Ichikawa K, Ichikawa H, Konda M, Murakami K (2009) Synoptic flow structures in the confluence region of the Kuroshio and the Ryukyu Current. J Geophys Res 114(C06007). doi:10.1029/2008JC005213

Nagano A, Ichikawa K, Ichikawa H, Tomita H, Tokinaga H, Konda M (2010) Stable volume and heat transports of the North Pacific subtropical gyre revealed by identifying the Kuroshio in synoptic hydrography south of Japan. J Geophys Res 115(C09002). doi:10.1029/2009JC005747

Nagano A, Ichikawa H, Yoshikawa Y, Kizu S, Hanawa K (2012a) Variation of the southward interior flow of the North Pacific subtropical gyre, as revealed by a repeat hydrographic survey. J Oceanogr 68(2):361–368. doi:10.1007/s10872-012-0102-3

Nagano A, Ichikawa K, Ichikawa H, Yoshikawa Y, Konda M, Murakami K (2012b) Subsurface current structures east of the Amami-Oshima Island based on LADCP observation. J Adv Mar Sci Technol Soc 18(2):19–26

Nagano A, Ichikawa K, Ichikawa H, Konda M, Murakami K (2013) Volume transports proceeding to the Kuroshio Extension region and recirculating in the Shikoku Basin. J Oceanogr 69(3):285–293. doi:10.1007/s10872-013-0173-9

Nitani H (1972) Beginning of the Kuroshio. In: Stommel H, Yoshida K (eds) Kuroshio—its physical aspects. University of Tokyo Press, Tokyo, pp 129–163

Oka E (2009) Seasonal and interannual variation of North Pacific subtropical mode water in 2003–2006. J Oceanogr 65:151–164

Oka E, Qiu B (2012) Progress of North Pacific mode water research in the past decade. J Oceanogr 68:5–12. doi:10.1007/s10872-011-0032-5

Okuda K, Yasuda I, Hiroe Y, Shimizu Y (2001) Structure of subsurface intrusion of the Oyashio water into the Kuroshio Extension and formation process of the North Pacific intermediate water. J Oceanogr 57:121–140

Qiu B, Chen S (2010) Interannual-to-decadal variability in the bifurcation of the North Equatorial Current off the Philippines. J Phys Oceanogr 40:2525–2538. doi:10.1175/2010JPO4462.1

Rainville L, Jayne SR, Cronin MF (2014) Variations of the North Pacific subtropical mode water from direct observations. J Clim 27:2842–2860. doi:10.1175/JCLI-D-13-00227.1

Suga T, Hanawa K (1995) The subtropical mode water circulation in the North Pacific. J Phys Oceanogr 25:958–970

Suga T, Takei Y, Hanawa K (1997) Thermostad distribution in the North Pacific subtropical gyre: the central mode water and the subtropical mode water. J Phys Oceanogr 27(1):140–152

Suga T, Kato A, Hanawa K (2000) North Pacific Tropical Water: its climatology and temporal changes associated with the climate regime shift in the 1970s. Prog Oceanogr 47:223–256

Sugimoto S, Hanawa K (2005) Remote reemergence areas of winter sea surface temperature anomalies in the North Pacific. Geophys Res Lett 32(L01606). doi:10.1029/2004GL021410

Sugimoto S, Takahashi N, Hanawa K (2013) Marked freshening of North Pacific subtropical mode water in 2009 and 2010:

influence of freshwater supply in the 2008 warm season. Geophys Res Lett 40:3102–3105. doi:10.1002/grl.50600

Taft B (1978) Structure of Kuroshio south of Japan. J Mar Res 36:77–117

Tomita H, Kubota M, Cronin MF, Iwasaki S, Konda M, Ichikawa H (2010) An assessment of the surface turbulent heat fluxes from J-OFURO2 at the KEO and JKEO sites. J Geophys Res 115(C03018). doi:10.1029/2009JC005545

Vivier F, Kelly KA, Thompson L (2002) Heat budget in the Kuroshio Extension region: 1993–99. J Phys Oceanogr 32:3436–3454